Surface waves in the Beaufort Sea

Madison Smith

A thesis
submitted in partial fulfillment of the
requirements for the degree of

Master of Science in Civil Engineering

University of Washington

2016

Committee:

Jim Thomson, Chair

Alex Horner-Devine

Erick Rogers

Program Authorized to Offer Degree:
Civil and Environmental Engineering

University of Washington

Abstract

Surface waves in the Beaufort Sea

Madison Smith

Chair of the Supervisory Committee:
Professor Jim Thomson
Civil and Environmental Engineering

The rapidly changing Arctic sea ice cover affects surface wave growth across all scales. The effect of sea ice extent on wave growth is studied using *in situ* measurements of waves observed from freely-drifting buoys during the 2014 open water season. Wave measurements made in open water areas of the Beaufort Sea are interpreted using open water distances determined from satellite ice products and wind forcing time series measured *in situ* with the buoys. A significant portion of the wave observations are found to be limited by open water distance (fetch) when the wind duration was sufficient for wind and wave conditions to be considered stationary. The scaling of wave energy and frequency with open water distance demonstrates the indirect effects of ice cover on regional wave evolution. Waves measurements in partial ice cover in the marginal ice zone (MIZ) can be similarly categorized as distance-limited by an 'effective fetch', representing the distance between ice floes, calculated by applying the fit from the open water scaling. The process of local wave generation in ice appears to be a strong function of the ice concentration, wherein the ice cover severely reduces the effective fetch. The wave field in the Beaufort Sea is thus a function of the sea ice both locally, where wave growth primarily occurs in the open water between floes, and regionally, where the ice edge provides a more classic fetch limitation. Observations of waves in recent years may be indicative of an emerging trend in the Arctic Ocean, where we will observe increasing wave energy with decreasing sea ice extent.

TABLE OF CONTENTS

LIST OF FIGURES

LIST OF TABLES

ACKNOWLEDGMENTS

Thanks to my committee, Jim, Alex, and Erick, for your valuable feedback and support. Thank you especially to Jim for your excellent mentorship. Thank you to the UW Environmental Fluid Mechanics group, and in particular my officemates, for your insight and camaraderie over the last two years.

Thanks to all who assisted in the collection and analysis of this data: the field engineers, Joe Talbert and Alex DeKlerk, designed, build and deployed the SWIFT drifters; the crews of the *R/V Ukpik* and *R/V Norseman II* assisted with deployment and recovery of SWIFTs 10 and 11; Craig Lee and the crew of the *R/V Araon* deployed SWIFT 15; Erick Rogers provided NAVGEM winds; Luc Rainville assisted with processing of ice products and satellite imagery; and Hans Graber and Alexis Denton at the University of Miami provided RadarSat2 images. This research was made possible by funding from the Office of Naval Research (N00014-12-1-0113) as part of the Marginal Ice Zone program. Additional funding for my first year of study was provided by the Valle Scholarship.

DEDICATION

At a recent meeting, wave modeler Gerbrant Van Vledder made a lovely metaphor from a characteristic of ocean waves: as waves age, energy is passed from higher frequencies to lower frequencies. This thesis is dedicated to those have have shared their energy, enthusiasm, and wisdom with me. To my parents, whose unparalleled support has carried me further than I ever knew I could go. Thank you.

PREAMBLE

This research builds on a recent paper (Thomson and Rogers, 2014) that used a 2012 dataset to show the applicability of fetch laws for scaling waves in the Arctic Basin. Their findings are updated by placing constraints on when limitation by open water distance is valid using a more spatially robust data set from 2014. Additionally, we propose a power-law relationship of the effective open water distance in partial ice with the ice concentration, which may be used to improve predictions of wave generation in ice.

The main body of this thesis has been published as an article in the Marginal Ice Zone special issue of Elementa (Smith and Thomson, 2016), and has been expanded here. The subsections that have been most notably expanded are in the Introduction (1.1, 1.2, and 1.3), the duration-limited condition results (3.3), and discussion of wave evolution (4.1). Additional figures included in this thesis are Figures 1.1, 1.2, 1.3, 1.4, 3.1(b), 3.2, 3.4, 3.5(a), and 4.2.

Chapter 1

INTRODUCTION

1.1 Describing a wave field

In the most basic sense, an ocean surface wave is a sinusoidal displacement of the free surface. The wave field in the ocean can be more accurately described as a superposition of sinusoidal waves of various sizes propagating in different directions (Figure 1.1, top), although it is in reality more complex than this. Description of the ocean surface, composed of waves of a range of heights, periods, and directions, is challenging. Scientists have formulated standard statistical methods to characterize complex wave fields in increasingly simple manners.

Based on the representation of the ocean surface as a superposition of sinusoids, Fourier analysis can be used to describe the surface displacement from average sea level, $\eta(t)$, as a summation of n cosine terms:

$$\eta(t) = \sum_{n} A_n \cos(\omega_n t + \phi_n) \tag{1.1}$$

where terms have distinct amplitudes (A), angular frequencies (ω), and phase (ϕ). The energy of each wave component is the square of the wave amplitude height, $E_n \propto A_n^2$.

Wave spectra can be developed to give a characterization of the distribution of wave energy across frequencies and directions at the ocean surface. Two-dimensional directional wave spectra and one-dimensional frequency spectra are commonly used for ocean wave measurements. The two-dimensional wave spectra allows the energy in the wave field to be expressed as a function of the frequency ($f = \frac{\omega}{2\pi}$) and direction of wave propagation (θ) corresponding to wave components. Here, the frequency is defined as the number of wave peaks that pass a point per second, and wave propagation direction follows the convention of measuring the direction waves come from (relative to 0° north). One-dimensional wave

spectra express the energy in the wave field as a function of frequency only.

The two-dimensional wave spectra, where $E(f,\theta)$ is the spectral energy density (Figure 1.2, bottom right), can be defined as:

$$E(f,\theta) = E(f)G(f,\theta) \tag{1.2}$$

where $E(f)$ is the one-dimensional frequency spectra and $G(f,\theta)$ is the directional spreading function. The spreading function has the properties of a probability density function, such that:

$$\int_0^{2\pi} G(f,\theta)d\theta = 1 \tag{1.3}$$

and can be expressed, similar to the sea surface above, as a fourier series of sinusoidal functions, where a_n and b_n are fourier coefficients:

$$G(f,\theta) = \frac{1}{\pi}\left[\frac{1}{2} + \sum_{n=1}^{\inf} a_n \cos n\theta + b_n \sin n\theta\right] \tag{1.4}$$

The one-dimensional frequency spectra, $E(f)$ in Equation 1.2 is an integration of the two-dimensional spectra over all directions. Here, the wave field is represented by the total energy density of all components at each frequency, without respect to direction (Figure 1.2, bottom left).

For ease of comparison, descriptions of wave fields are often further simplified into bulk parameters that statistically summarize the dominant wave signal. The characteristic period of the wave field, where the period is the time between wave peaks passing a fixed point, can be calculated in a number of ways. In general, the period is calculated as the inverse of the frequency, $T = \frac{1}{f}$. Then, the peak period, T_p, is simply the inverse of the frequency in the one-dimensional wave spectra where the most energy is concentrated. The energy-weighted period is defined as $T_e = \frac{m_0}{m_1}$, where $m_n = \int E(f)\, f^n\, df$. This metric is often preferable to capture a range of periods in the wave field. Significant wave height has been traditionally defined as the mean wave height, crest to trough, of the largest third of the waves, defined as such to agree historical records of wave height from visual observations

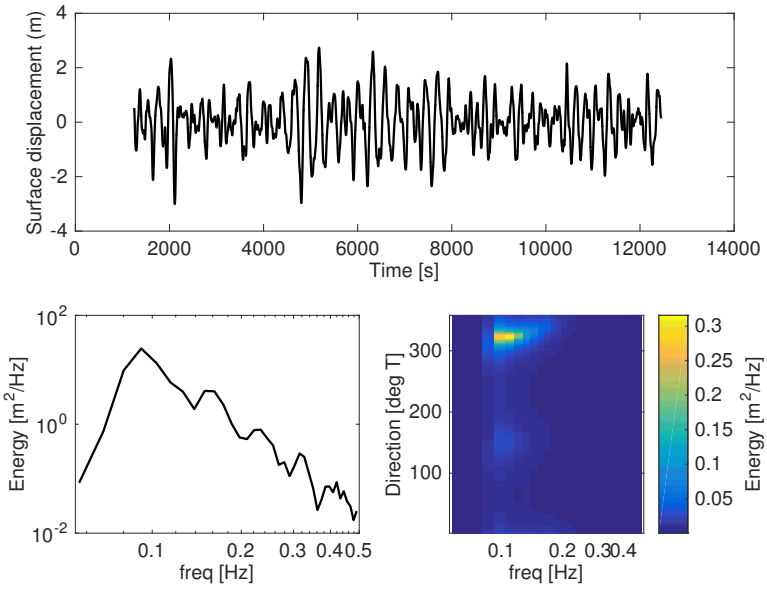

Figure 1.1: Example of wave spectrum generated from a time series of sea surface displacement reconstructed from a wave buoy in the Beaufort Sea, October 2, 2015 (top). One-dimensional frequency spectra (bottom left) shows energy distribution as a function of frequency only and two-dimensional directional spectra (bottom right) gives energy distribution as a function of both frequency and direction. Here, the wave energy peaks at 0.1 Hz (corresponding to a period of 10 seconds) and a direction of 330°.

before wave measurements were prolific. In practice, significant wave height is calculated statistically as four times the square root of the zeroth-moment of the frequency wave spectra, m_0 (i.e., the area under the frequency wave spectra), or $H_s = 4\sqrt{m_0}$.

The wave age is a useful metric for characterizing a wind-generated wave field, defined as the ratio of the wave phase speed to the wind speed, c_p/U_{10}, where the wave phase speed is $c_p = \frac{gT_e}{2\pi}$. The wave age ratio indicates how strongly the local wind is forcing the waves. When the age is small ($c_p/U_{10} < 1$), local winds are strongly driving the wave field and waves are considered young. When the wave age is large ($c_p/U_{10} > 1$), waves are considered relatively old and mature, and are often referred to as swell waves.

1.2 Ocean wave generation

Ocean surface waves are generated by winds acting over the sea surface, which requires both time and distance to develop. The wave field then depends strongly on the characteristics of the wind field, including its direction, speed, and variation. However, the development of the wave field is often limited by either the time the wind has blown for, or the distance of the ocean it has blown over (commonly known as the fetch), leading to two idealized cases of wave growth: duration-limited growth, and distance- (or fetch) limited growth. Although this simplistic categorization does not account for the unsteady winds commonly observed *in situ*, the two idealized cases provide valuable insight into the physical process of wave evolution. Wave evolution as a function of distance and duration are often described using nondimensional variables for wave energy, wave frequency, open water distance, and wind duration:

$$\tilde{E} = \frac{g^2 H_s^2}{16 U^4} \tag{1.5}$$

$$\nu = \frac{U f_e}{g} \tag{1.6}$$

$$\mathcal{X} = \frac{gx}{U^2} \tag{1.7}$$

$$\varsigma = \frac{gt}{U} \tag{1.8}$$

where g is gravitational acceleration, H_s is significant wave height, U is wind speed (commonly taken at ten-meter height, U_{10}), f_e is energy-weighted average frequency, x is dimensional open water distance, and t is wind duration (Young, 1999).

1.2.1 Distance-limited wave growth

The idealized case for distance- (or fetch-) limited growth occurs when a constant wind blows perpendicular to and away from a coastline for a sufficiently long period of time such that the wave characteristics have equilibrated. Here, the wave field is a direct function of the distance from the coast, i.e. $\tilde{E} = f(\mathcal{X})$ and $\nu = f(\mathcal{X})$, where the same wind generates larger and lower frequency waves as the fetch increases (Figure 1.2).

Empirical studies in lakes and the coastal ocean have shown that wave energy and frequency scale well with generation distance across a range of conditions, with exponential relationships of the form $\tilde{E} = A\mathcal{X}^a$ and $\nu = B\mathcal{X}^b$. Results from the JONSWAP experiment in the North Sea are still held as one of the most classic examples of a true fetch-limited experiment, with wave measurements taken at multiple sites along a transect (Hasselmann, 1973). These results were augmented with other field and laboratory data to find fetch relations of $\tilde{E} = 1.6 \times 10^{-7}\mathcal{X}^1$ and $\nu = 3.5\mathcal{X}^{-0.33}$. Similarly, a fetch limitation experiment in Lake Ontario gave fetch relations of $\tilde{E}= 8.415 \times 10^{-7}\mathcal{X}^{0.76}$ and $\nu = 1.85\mathcal{X}^{-0.23}$ (Donelan et al., 1985). Numerous other studies both in the field and laboratory have reexamined these fits with consistent results; values of A range from 1.6×10^{-7} to 1.3×10^{-6}, and values of a range from 0.75 to 1.00 (Young, 1999). Similarly, fetch relations fit to field data of nondimensional wave frequency (ν) with nondimensional distance give coefficients B of 2.41 ± 0.19 and b of 0.275 ± 0.16 (Babanin and Soloviev, 1998).

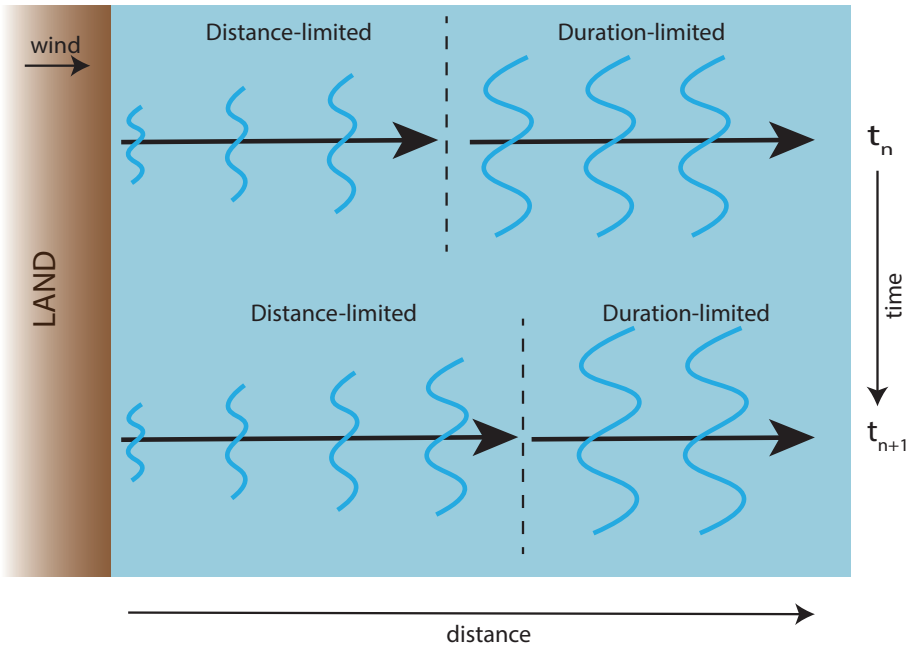

Figure 1.2: Schematic of idealized cases of distance-limited and duration-limited growth. At time t_n (top), a wind blowing perpendicular away from the coast will generate waves by distance-limited growth, then duration-limited growth. At time t_{n+1} (bottom), the duration has increased, such that distance-limited growth extends further from the coast, and duration-limited waves have grown.

Basic fetch laws have been expanded on in recent years in order to model wave generation more precisely and in more complex environments. The evolution of the wave frequency spectra with increasing distance was originally noted by Donelan et al. (1985) and has been confirmed by many other field studies (e.g. Young and Verhagen, 1996; Schwendeman and Thomson, 2014). Theoretical modeling of fetch-limited wind wave growth assumes that wave groups evolve independently, where wind pumping and dissipation by breaking are in equilibrium (Fontaine, 2013). Recent work has sought to improve wave predictions beyond the basic development of the wind-wave spectra by considering nonstationary energy transfer and wave group processes (Liu et al., 2002). Additionally, two-dimensional spectral predictions have been improved by the finding that high frequency waves in a fetch-limited limited sea will have a bimodal directional distribution (Ewans, 1998).

1.2.2 Duration-limited wave growth

The idealized case for duration-limited growth begins with a calm sea and a sufficiently large expanse of open water for no distance limitation to occur. A steady wind that is fast enough to cause significant drag on the ocean surface, over about 5 m/s, will cause wave height to gradually increase (Young, 1999). Then, the wave field will be a function of only the wind duration, i.e. $\tilde{E} = f(\varsigma)$ and $\nu = f(\varsigma)$. Ocean waves outside of the coastal region are generally thought to be mostly duration-limited, as a result of the large distances available for wave generation (Figure 1.2).

However, there are few sets of truly duration-limited ocean wave data, as natural winds are rarely constant for a significant period of time (Stewart, 1961; Sanders, 1976). To this day, the primary duration-limited wave records cited and used in the literature are those from the early results of Sverdrup and Munk (1947), Bretschneider (1952), and Darbyshire (1959). Due to the difficulty of obtaining duration limited wave results, Bretschneider (1952) proposed a conversion for well-studied fetch-limited power laws in order to study duration-limited wave growth. These conversions have been improved by further work (Mitsuyasu and Rikiishyi, 1978; Hwang and Wang, 2004; Hwang, 2006), but the description of duration-

limited waves remains remarkably unresolved.

1.2.3 Transition from distance to duration limitation

Although these two endpoints for types of wave generation appear theoretically distinct, determining a cutoff to distinguish between the two is challenging. Based on the idealized descriptions of distance and duration limited growth, the distance at which duration-limited growth occurs should increase as the duration becomes larger (Figure 1.2). Thus, the transition from distance- to duration-limited growth should depend on both the open water distance and the wind duration. A formula relating the nondimensional distance and duration in this way was first proposed in 1977, based on empirical data, as (CERC, 1977):

$$\varsigma = 6.5882 \exp[0.0161 \, (\ln\mathcal{X})^2 - 0.3692 \ln\mathcal{X} + 2.2024]^{1/2} + 0.8798 \ln\mathcal{X} \tag{1.9}$$

The implications of this equation are expressed graphically in Figure 1.3.

A few years later, an alternative empirical formula for the time required for wave generation to become duration limited was proposed:

$$t_{required} = 77.3 \frac{\mathcal{X}^{0.67}}{U^{0.34} g^{0.33}} \tag{1.10}$$

where duration limitation occurs when measured wind duration, t, is greater than $t_{required}$. In both of these empirical formulas, as well as others that have been proposed, the distance over which waves are considered fetch or distance limited increases as the wind duration increases. However, while the wind duration appears as a clearly defined value in the idealized case presented, it is much trickier to define from the complex, nonstationary wind fields that occur in reality.

There have been a number of proposed metrics to determine wind duration, t. The simplest method is a "zero-crossing" style approach, where the duration is the time since the wind has been less than 5 m/s (Young, 1999). Alternatively, the duration can be defined using the open water distance, x, as the time necessary for a wave group to travel from the

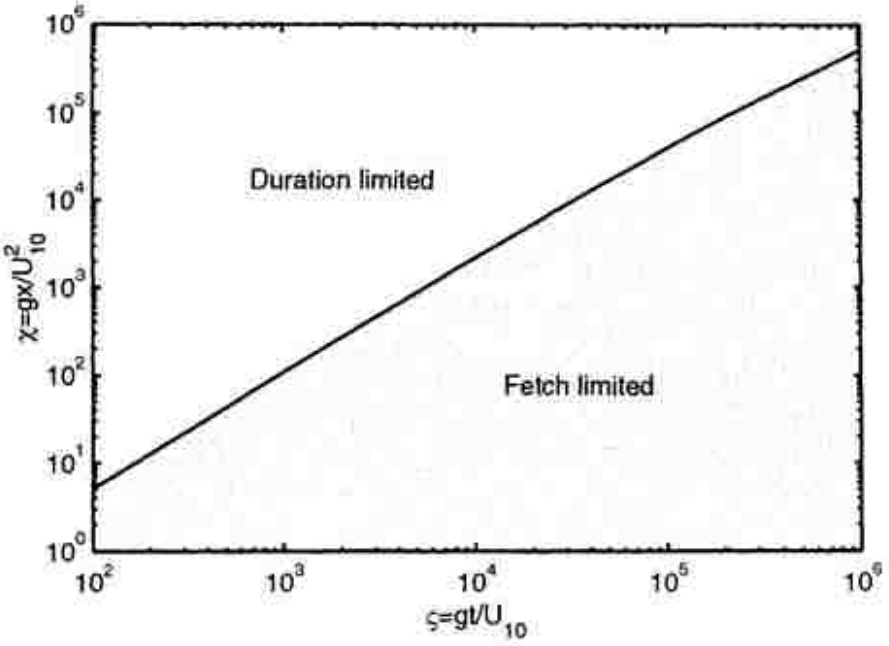

Figure 1.3: Relation of the nondimensional fetch and nondimensional duration, resulting from Equation 1.9. Data which maps above the line represents duration-limited growth, while data which maps below the line represents fetch-limited (or distance-limited) growth. (Young, 1999)

upwind boundary to the location of measurement (Mitsuyasu and Rikiishyi, 1978):

$$t = \int_0^x (c_g)^{-1} dx \tag{1.11}$$

where c_g is the wave group velocity. However, these metrics often fail to capture the complexities of wind patterns. In reality, many ocean waves are limited by both distance and duration. Only a few studies have examined duration-limited waves under either precise field conditions or in the laboratory, and even less have examined waves simultaneously limited by both distance and duration (Hwang and Wang, 2004).

In the polar regions, fetch limitation can be caused by not only land, but by sea ice. Wave generation is expected to then be a function of both open water distance and wind duration, as well as the extent of the sea ice cover.

1.3 Observations of waves in sea ice

The average summer sea ice extent in the Arctic Ocean has significantly decreased in recent decades. In fact, the previously perennial Arctic sea ice cover may now be entering a seasonal regime comparable to that of the Antarctic (Martin et al., 2014). Wave energy and period in the Beaufort Sea region have increased during the open water season as a result, representing a transition towards swell-dominated wave conditions (Wang et al., 2015). We expect conventional fetch laws to apply in the open waters of the Arctic Ocean, where open water distance may be from either land or the ice edge. Then, with increasing open water area, larger and longer waves will evolve under the same wind conditions. An unprecedentedly large wave event was measured in the Beaufort Sea in 2012, with significant wave height reaching five meters (Thomson and Rogers, 2014). The increase of wave energy in the partially ice-covered Arctic Ocean, particularly during such storm events, may contribute to the further breakup of sea ice (Kohout et al., 2014). This feedback accelerates the predicted timeline to an ice-free Arctic summer, and motivates study of the dependence of Arctic Ocean surface waves on sea ice coverage.

The marginal ice zone (MIZ) is the dynamic region near the edge of the ice pack where

there is a mixture of ice floes, open water, and brash ice. Wave energy in this region is highly variable; wave heights are generally reduced from the open water, but large waves may persist. Wave attenuation by sea ice encompasses the exponential decay of wave energy through a variety of physical processes in the MIZ (Wadhams et al., 1988). The attenuation rate is a function of the ice cover characteristics (concentration, floe size distribution, and thickness) as well as the wave frequency. High frequency waves are attenuated rapidly while low frequency waves are able to penetrate further with minimal attenuation. Recent work has found that storm waves in the Arctic Ocean can propagate further into the ice than previously believed, as a result of nonlinear energy transfer to lower frequencies (Li et al., 2015).

The penetration of waves from open water into the MIZ, including the dissipation and scattering of waves that cause wave attenuation, has been a focus of research for many years (Squire et al., 1995; Squire, 2007, and references therein). Dissipation is the dominant process when the sea ice cover can be considered to be a viscous medium, as is true with frazil or pancake sea ice. Scattering through the partial reflection of incoming waves is the dominant process when the sea ice is continuous or with large floe size diameters. Recent models for wave-ice interactions have attempted to reconcile attenuation resulting from both processes in a complex MIZ, but are still far from reliably predicting future wave conditions (Wang et al., 2015).

Additionally, waves can be generated locally by winds within partial ice cover. Masson and LeBlond (1989) used a basic numerical model to explore how the two-dimensional wavenumber spectrum develops and evolves in partial ice cover. Their model uses the energy balance equation (Hasselmann, 1960):

$$\frac{\partial F(f,\theta;\mathbf{x},t)}{\partial t} + C_g(f,\theta)\cdot\nabla F(f,\theta;\mathbf{x},t) = S_{in} + S_{ds} + S_{nl} + S_{ice} \tag{1.12}$$

where $F(f,\theta;\mathbf{x},t)$ is the directional frequency energy spectrum evolving in time and space, $C_g(f,\theta)$ is the group velocity, S_{in} is the energy input rate, S_{ds} is the dissipation rate, and S_{nl} is the nonlinear transfer of energy. This equation is altered for the partial ice cover of

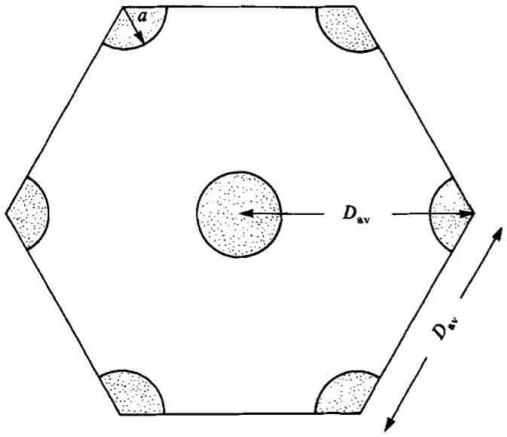

Figure 1.4: Simple model of fetch-limited wave generation in homogenous partial ice cover formulated by Masson and LeBlond (1989). Here, an ice field with ice cover f_i and average floe radius a is assumed to have an approximate distance between floes of D_{av}.

the MIZ by assuming the energy input and dissipation terms, S_{in} and S_{ds}, to be linearly scaled based on the percent of open water$(1 - f_i)$, where f_i is the fraction of ice cover. S_{ice} is determined using a simple potential flow theory model for scattering and dissipation by ice floes. Scattering is treated as a combination of motion generated by an oscillating floe and the motion generated by the reflection of incident motion for each floe. The result is then integrated over the entire ice field by assuming a hexagonal model with homogenous ice cover, where the average distance between floes is D_{av} and the average floe radius is a (Figure 1.4). The degree of ice cover is summarized as:

$$f_i = 2\pi a^2 \sqrt{3D_{av}^2} \tag{1.13}$$

This model and relation can similarly be used to calculate the relevant fetch length between floes, D_{av}, based on the fraction of ice cover and characteristic floe size. In this model, energy at low frequencies is quickly scattered and becomes isotropic, while energy at high frequencies attenuates more slowly due to other source functions in partial ice.

In applying this simple model to a non-zero initial wave field, Masson and LeBlond (1989)

found that short, fetch-limited wave growth occurs in partial ice cover, but of a relative magnitude that they considered insignificant compared to open water wave generation. Since this early study of wave generation in ice, there has been little research revisiting this subject. Recent research has shown that the energy balance equation (Equation 1.12) is more complexly altered by partial ice than represented here (Zippel and Thomson, 2016; Martin et al., 2016). The wind input term is reduced in partial ice, as the energy transferred from wind to the waves depends on the waves. The reduction of the input from wind then creates a feedback loop that explains the decreased wave generation in the MIZ (Zippel and Thomson, 2016). However, much is still unknown about wave generation and growth in partial ice cover (Squire, 2007).

A recent paper showed that nondimensional scalings of wave energy with open water distance apply for much of the 2012 open water season in the Beaufort Sea region, such that wave generation can be considered distance-limited (Thomson and Rogers, 2014). Here, we use a new data set (2014) to explore the nuances of distance limitation with improved temporal and spatial coverage. In particular, we examine the constraint of waves by sea ice, including analysis of ice-limited wave growth in partial ice cover. The wave measurement and calculation of open water distances are described below. We then present results and analyses, and discuss wave evolution and our reanalysis of the 2012 data set used in Thomson and Rogers (2014).

Chapter 2

METHODS

2.1 Data collection

Wave data were collected in the Beaufort Sea during the 2014 open water season using three Surface Wave Instrument Floats with Tracking (SWIFTs). SWIFTs are freely-drifting buoys that collect observations in ten-minute bursts at the top of each hour, and burst results are transmitted hourly via Iridium satellite antenna. SWIFTs 10 and 11 were deployed on July 27 from the *R/V Ukpik* roughly 100 km north of Alaska. They followed approximately the same path until September 1, when SWIFT 10 was caught in partial ice cover until September 15. Both buoys were recovered from the *R/V Norseman II* September 28-29, 2014. SWIFT 15 was deployed and recovered from the *R/V Araon* from August 5 to 17, 2014, and was in partial ice cover the entirety of its deployment. Drift tracks of the SWIFTs are shown in Figure 2.1.

The wave-following reference frame of the SWIFT buoy allows wave spectra to be obtained from ocean surface velocities. The motion of the platform is measured using a GPS receiver (Microstrain 3DM-GX3-35) at 4 Hz, with a horizontal velocity precision of 0.05 m/s. Horizontal velocity vectors are decomposed into mean and wave orbital velocity components that are used to infer wave energy spectra (Herbers et al., 2012; Thomson, 2012). The natural frequency of the buoy, with a period of 1.3 seconds, is damped by a small heave plate to allow observations of wave motions from low frequency swells to high frequency wind waves. Wave energy spectra were calculated from ensemble averaging of the fast Fourier transform (FFT) with an overlap of 50%. Significant wave height (H_s) and energy-weighted average period (T_e) were obtained from the wave energy spectra. Significant wave height was determined in the frequency domain as four times the square root of the zeroth-moment of the

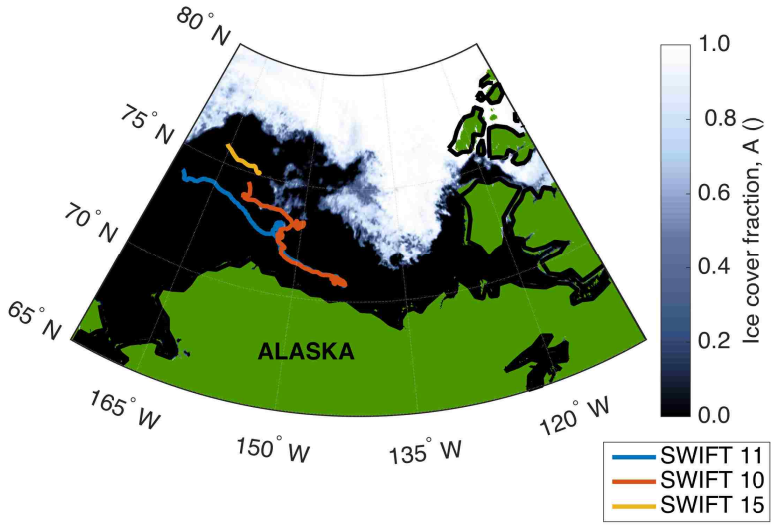

Figure 2.1: Tracks of SWIFT drifters in the Beaufort Sea. Thick colored lines mark the tracks of SWIFTs 11 (blue), 10 (red), and 15 (yellow). SWIFTs 11 and 10 were deployed from July 27 to September 29, and SWIFT 15 was deployed from August 5 to 17. Shown over fraction of sea ice cover on September 1, A, from AMSR2 sea ice product (Beitsch et al., 2013).

wave spectra, (m_0; i.e., the area under the wave spectra), or $H_s = 4\sqrt{m_0}$. Energy-weighted average period was determined as $f_e = \frac{m_1}{m_0}$. Nondimensional wave energy and frequency were determined from Equations 1.5 and 1.6.

Wind speed, wind direction, and air temperature were collected at 1-meter mast height with an Airmar PB200 ultrasonic anemometer. Wind speeds were corrected to ten-meter wind speeds (U_{10}) by assuming a logarithmic profile, where $U_{10} = 1.35U_1$ (Benschop, 1996). Turbulent velocity profiles were measured using either a down-looking or High Resolution up-looking Nortek Aquadopp Doppler profiler in the lower hull. Additionally, photos were taken at 0.25 Hz during data collection bursts from a mast-mounted uCAM serial camera. A more detailed description of the SWIFT platform can be found in Thomson (2012). Time series of measured wind speed, significant wave height, energy-weighted period, and peak wave direction are shown in Figure 2.2. The anemometer and lower hull were lost from SWIFT 10 on September 15 as it exited the ice. As wind speed and wave directions are missing after this time, Navy Global Environmental Model (NAVGEM) wind speeds and wave direction were used instead (Hogan et al., 2014) and are differentiated in the figure by stars.

2.2 Open water distance estimates

Open water distances were estimated using a branched approach, differentiating between distances measured in areas of open ocean and partial ice cover. Images from the camera onboard the SWIFT were used to determine whether measurements were taken in ice-free or partially ice-covered ocean (see Figures 2.3 and 2.4). Timelapse videos made from these images during the observations of SWIFT 10 and SWIFT 15 in partial ice are available online (http://faculty.washington.edu/jmt3rd/SWIFTdata/ArcticOcean/SWIFT10_Sep1_Sep15_Timelapse_rotated.mov and http://faculty.washington.edu/jmt3rd/SWIFTdata/ArcticOcean/SWIFT15_Aug6_Aug18_Timelapse.mp4, respectively).

When the onboard SWIFT images confirmed the absence of sea ice locally, open water distances were estimated using the daily 4 km National Ice Center's (NIC) Multisensor Snow

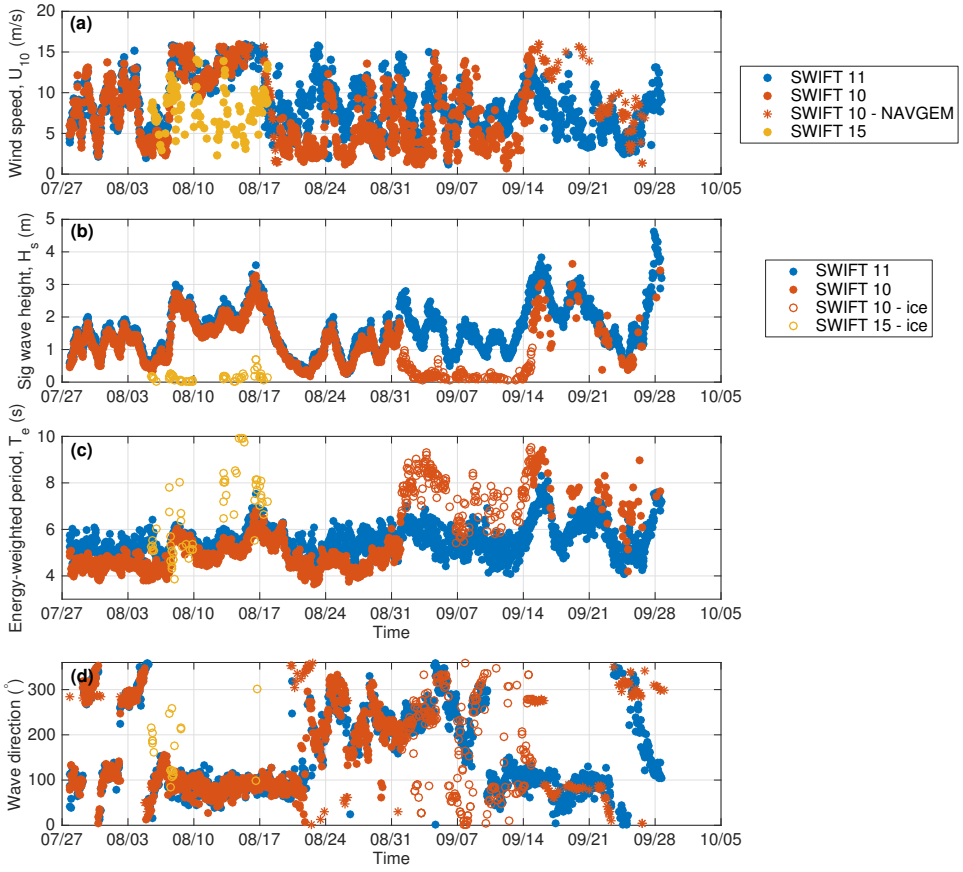

Figure 2.2: Time series of sea surface measurements during 2014 open water season from SWIFTs: (a) wind speed corrected to 10 m, (b) significant wave height, (c) energy-weighted wave period, and (d) peak wave direction (from 0 degrees North). Stars indicate winds from NAVGEM model outputs. Open circles indicate wave measurements made in partial ice cover.

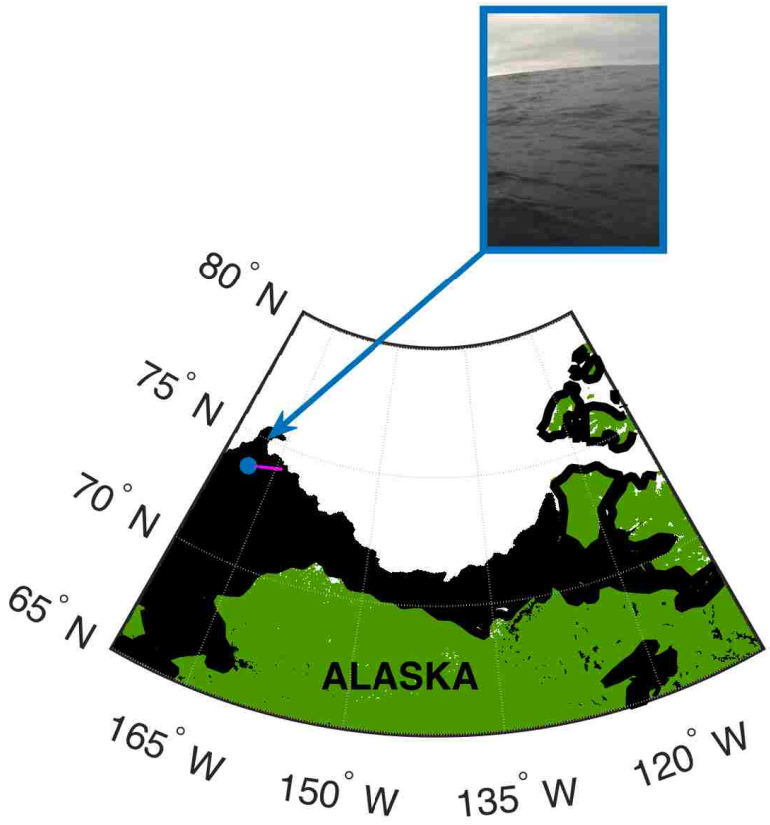

Figure 2.3: Example calculation of open water distance (fetch) for SWIFT 11 on September 24. Image taken from SWIFT confirms no local ice cover. Ice extent from NIC IMS product was used to calculate distance to the ice edge (magenta) in the peak wave direction. Here, fetch is $x = 34$ km.

and Ice Mapping System (IMS) product, which uses a threshold of 15% ice concentration to determine the presence of ice (National Ice Center, 2008). The IMS product is produced from a human analysis of all available satellite image products, including visible, passive microwave, synthetic aperture radar (SAR), and radar scatterometer images, as well as snow mapping algorithms and other ancillary data, in order to give a relatively high resolution view of Arctic sea ice on a given day. The open water distance was calculated as the distance along the peak wave direction from the buoy to a land or ice boundary (Donelan et al., 1985). An example of the estimation of distance is shown in Figure 2.3 for SWIFT 11 on September 24, where the magenta line is the open water distance, $x = 34$ km. The nondimensional open water distance ($\mathcal{X}$) was then calculated using Equation 1.7. The relationship of nondimensional wave energy ($\tilde{E}$; Equation 1.5) and nondimensional open water distance in the Beaufort Sea was obtained using a least squares regression to the data.

2.3 Wind duration estimates

Estimates of wind duration, t, were made using the "zero crossing" approach by calculating the cumulative sum of time that wind speed has been above 5 m/s. The wind speed at 10-meter height, U_{10}, was calculated from the SWIFT wind record, shown in Figure 2.2. The wind duration is reset to zero when the wind speed drops below 5 m/s, as this is considered the minimum for wave growth. For wind speeds less than 5 m/s, duration of 0 is used.

2.4 Wave measurements in partial ice

When partial ice is indicated by the SWIFT photos, wave measurements are considered to be in ice. The nondimensional energy of waves in partial ice is calculated using measured significant wave heights and wind speeds, as in Equation 1.5. The least squares regression relating nondimensional energy to nondimensional distance in open water can then be applied to find 'effective' nondimensional distance, $\mathcal{X}_{ice}$. A dimensional 'effective' distance for wave generation in the ice, x_{ice}, can be found using Equation 1.7.

2.5 Ice concentration estimates

Calculated nondimensional wave energy in partial ice, $\tilde{E}$, were interpreted using the local percent ice concentration. The Advanced Microwave Scanning Radiometer 2 (AMSR2) passive microwave daily product from the University of Bremen (Beitsch et al., 2013), generated at a 6.25 km resolution using the ASI ice algorithm, was used to estimate ice cover as an average of all non-zero ice concentrations within a 30-km radius of the SWIFT location. Although the small field of view and low image resolution make it impossible to determine ice concentration from the onboard SWIFT images, they were used to qualitatively validate AMSR2 estimates. Figure 2.4 illustrates the estimation of ice concentration using AMSR2, with validation from the SWIFT image. We were also able to obtain concentrations from high-resolution Radarsat-2 (RS2) images for two cases in which images were collocated with SWIFT 10 in partial ice. RS2 images were thresholded with a level of 0.1 to separate ice floes from open water, and the portion of ice floes in a 30-km radius of the SWIFT calculated. Error estimates in ice cover fraction were calculated as the standard deviation of ice concentration within the 30-km radius.

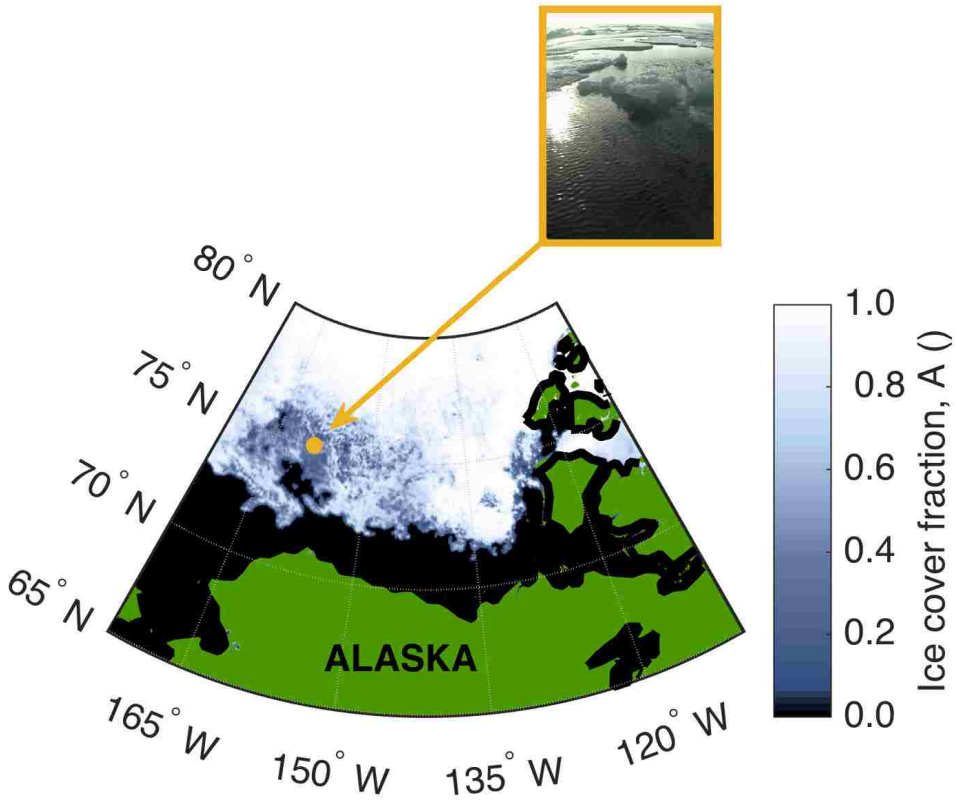

Figure 2.4: Fraction of local sea ice cover, A, from AMSR2 for SWIFT 15 on August 6. Local ice concentration was determined by averaging nonzero ice concentrations within a 30-km radius of SWIFT. Here, local ice concentration was calculated as 0.60. Image taken from SWIFT qualitatively confirms this estimate.

Chapter 3

RESULTS AND ANALYSES

The time series of winds and waves in Figure 2.2 show the range of conditions observed throughout the study period. Local ten-meter winds (Figure 2.2a) varied from just under 1 m/s to nearly 15 m/s. A few nonphysical wind measurements were removed in quality control. Two notable storms were captured, in early August and late September. Maximum wave heights (Figure 2.2b) occurred on September 28, at the end of the September storm, with a peak significant wave height of 4.6 m measured by SWIFT 11. Wave heights during the early August storm reached nearly 4 m. The wave characteristics from SWIFTs 10 and 11 roughly paralleled each other until September 1, when SWIFT 10 entered the MIZ (Figure 2.1). SWIFT 10 was in partial ice cover during the first two weeks of September, and SWIFT 15 was in ice the entirety of its mid-August deployment. These ice conditions were confirmed by the SWIFT onboard images. Wave characteristics measured in partial ice (indicated in the figure by open circles) have noticeably reduced significant wave heights and increased wave periods. Energy-weighted wave period in ice-free regions fluctuates between about 4 and 7 seconds, and reaches nearly 10 seconds in the ice (Figure 2.2c). Peak wave direction (Figure 2.2d) is primarily clustered around 100°, or approximately from the east.

3.1 Data screening

We initially attempted to separate out distance- and duration-limited wave measurements conditions using the definitions for the time required as a function of fetch, defined in Equations 1.9 and 1.10. Both equations did a poor job of separating out the type of wave growth, as measured by the regression of wave energy with open water distance, due to the failure of the wave duration variable to capture the complexity of the wind field.

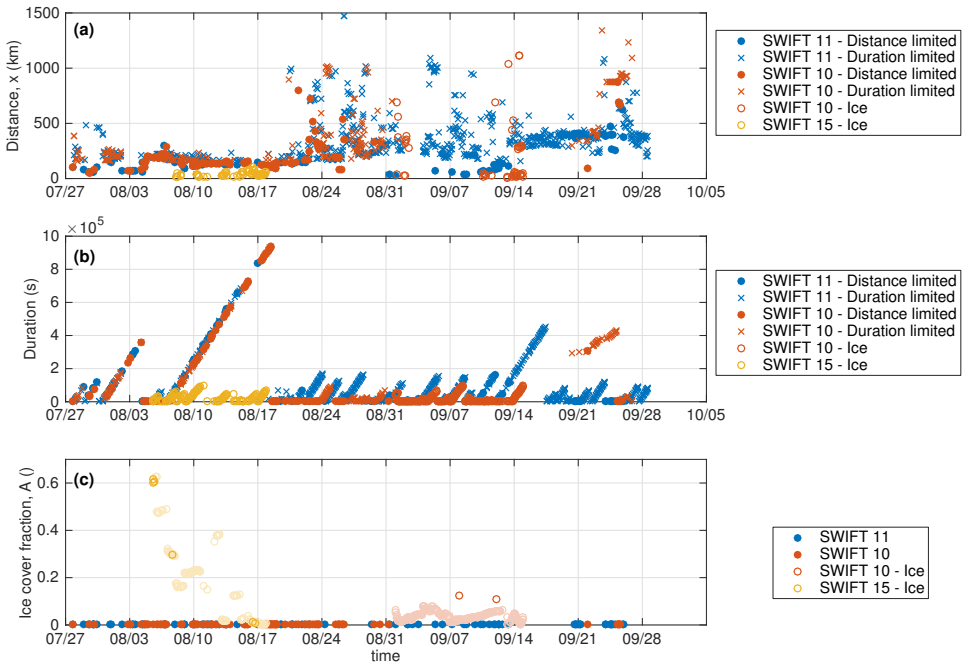

Figure 3.1: Time series of (a) calculated open water distances, x, (b) wind duration, and (c) fraction of sea surface that is ice-covered, A. All open water distances calculated using NIC IMS ice product are shown, with duration-limited waves indicated by x's, distance-limited waves indicated by filled circles, and waves in ice indicated by open circles. Ice cover is shown for all wave measurements. Nonzero ice concentrations, indicated by open circles, were determined primarily from AMSR2 product, with a few from RS2 for SWIFT 10. Ice concentrations that have been qualitatively validated by SWIFT images and correspond to off-ice winds are opaque, while ice concentrations that disagree with images or correspond to unsteady or on-ice winds are transparent.

We used an empirical approach based on the descriptions of ideal duration- and distance-limited wave growth to screen wave data. Duration-limited waves are likely when there is a large distance for wave generation and local wind speed greater than 5 m/s. When winds are below 5 m/s, waves are more likely to be fully developed. From the remaining waves, distance limitation is most likely for waves with relatively stable wind speed and wave height. We empirically determine cutoff values for minimum open water distance and maximum rate of change of wind speed and wave height by maximizing the coefficient of the least squares regression fit of nondimensional fetch versus nondimensional energy for distance-limited waves (discussed below; Figure 3.3b).

The resulting coefficients of determination for the distance scaling as a function of each screening parameter are shown in Figure 3.2, where we have not applied any other screening for each. As the distance-limited wave scaling is maximized when distances over 160 km are excluded (Figure 3.2, left), we determine that waves with open water distance greater than 160 km and local wind speed greater than 5 m/s are likely duration limited (indicated in Figure 3.1 by x's). After removing duration-limited waves, distance-limited waves are most likely when winds are stationary such that the wind speed is changing by less than 0.12 m/s h^{-1} (Figure 3.2, middle) and when the wave field is stationary such that significant wave height is change by less than 0.3 m h^{-1} (Figure 3.2, right; indicated in Figure 3.1 by filled circles). Cases with wind speed less than 5 m/s can be categorized as either unsteady or fetch-limited; although the majority are categorized as unsteady. Of the 1680 hourly measurements of waves in ice-free ocean, 52% were categorized as duration-limited and 22% were categorized as unsteady, with the remaining 26% expected to be purely distance-limited (Table 3.1). As the sea ice retreated towards September, wave growth was distance-limited less often and duration-limited more often (Figure 3.1).

3.2 Open water distance-limited conditions

Time series of dimensional open water distances derived using NIC IMS ice extents is shown in Figure 3.1a. Here, we show distances for both distance- and duration-limited wave conditions;

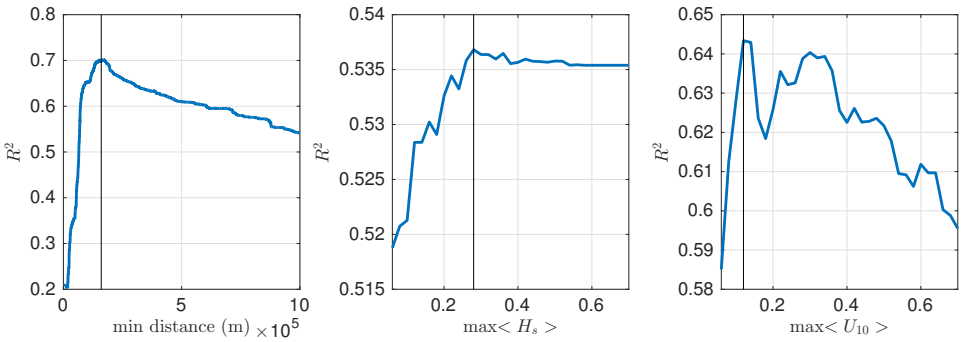

Figure 3.2: Fit of the distance-limited wave energy scaling, indicated by the R^2, as a function of three screening parameters (from left to right): minimum open water distance for waves to be duration-limited, maximum change in wind speed for waves to be distance-limited, and maximum change in wave height for waves to be distance-limited. All fits were determined for only open water waves where no other screenings have been applied. Horizontal black lines indicate chosen screening value.

duration-limited results are indicated by x's, and distance-limited results are indicated by circles. The seasonal cycle of ice retreat and advance is evident, as open water distances increased towards mid-September and then began to decrease. This cycle corresponds with the measured minimum sea ice extent in this region, on September 16 (Fetterer et al., 2002). Additionally, the period of lowest ice extent corresponds to the greatest variability in open water distance.

In Figure 3.3, we present scalings of wave energy with open water distance. The scaling on the left (Figure 3.3a) includes all waves in open water, prior to the data screening as described above (i.e., 100% of the data set). The slope of the fit is $\mathcal{X}^{0.88}$, with the coefficient of determination $R^2 = 0.64$. A majority of the points with the largest errors are from the end of August, when there were large changes in wind speed and open water distance over short time scales. Nonstationarity in conditions results in poor correlation between open water distance and wave energy.

The scaling of wave energy with open water distance for distance-limited waves only, as

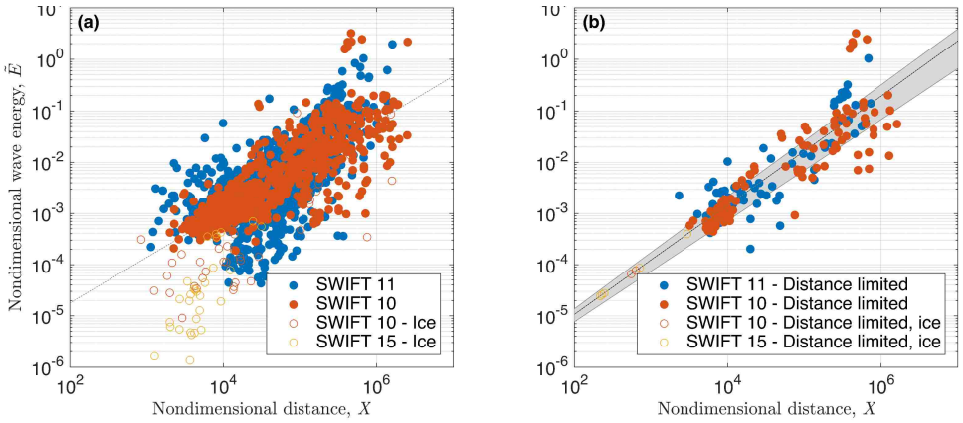

Figure 3.3: Scalings of waves in the Beaufort Sea with open water distance. (a) Scaling including all waves measured hourly by SWIFTs, with corresponding open water distances from Figure 3.1a. Dashed line is regression by least squares, with slope of $\mathcal{X}^{0.88}$. (b) Scaling using only distance-limited waves from open water. Black line is regression with slope $\mathcal{X}^{0.98}$, and associated normalized root-mean-square error (NRMSE) is shaded grey region. Distance-limited waves in partial ice (Figure 3.1b) are plotted on line as open circles using measured energy to infer the associated nondimensional distance required for generation.

screened using the empirically determined cutoffs above (Figure 3.2), are shown in Figure 3.3b. Comparing the scaling of the unscreened data in (a) to the scaling of the screened data in (b) shows significant improvement in the fit of the fetch law. The least squares regression fit to the distance-limited subset of the data (b) is:

$$\tilde{E} = 1.7 \times 10^{-7} \mathcal{X}^{0.98} \tag{3.1}$$

with a coefficient of determination of $R^2 = 0.79$. This fit is in agreement with canonical ones, where the exponent typically ranges from 0.75 to 1.00 (Young, 1999). Nondimensional variables calculated with NAVGEM model winds, at the end of SWIFT 10's deployment, scattered well with the rest of the data and negligibly changed results.

The strength of this scaling supports the dependence of wave energy flux in the Beaufort Sea on sea ice extent, as observed in 2012 (Thomson and Rogers, 2014). Scaling analysis such as this is susceptible to spurious correlation, due to the presence of U_{10} in all nondimensional variables. We find a spurious correlation of $R^2 = 0.37$ when a random number generator is used for distances. The spurious correlation is primarily due to the correlation between wind speed and wave height, and confirms that the correlation of distance with wave energy is in fact significant.

3.3 Duration-limited conditions

Dimensional wind durations, in seconds, are shown in Figure 3.1b. Duration-limited results are indicated by x's, and distance-limited results are indicated by circles. Empirical determination of duration- and distance-limited waves indicated that duration-limitation is likely when open water distances exceed 160 km, and wind speeds are greater than 5 m/s. These conditions represent 52% of our wave measurements in ice-free ocean.

However, wind duration estimates calculated using commonly defined methods do not well describe duration-limited wave growth. In Figure 3.4, we present nondimensional scalings of wave energy with wind duration. The scaling in Figure 3.4a includes durations for all wave measurements in open water, prior to data screening, while the scaling in Figure 3.4b

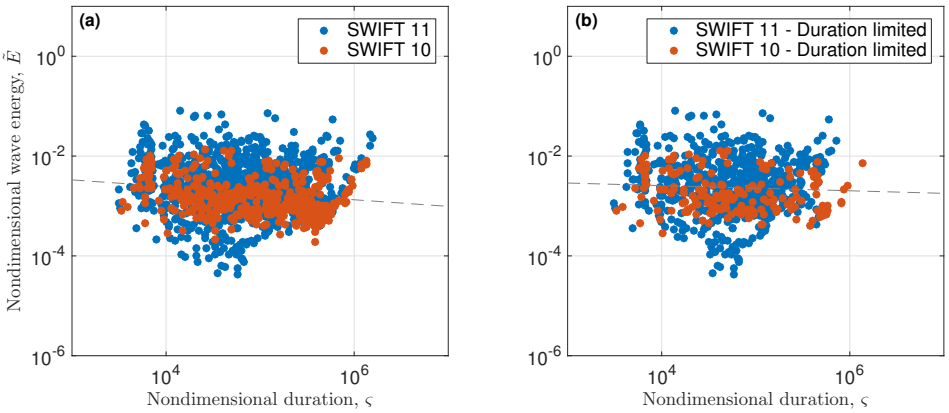

Figure 3.4: Scalings of waves in the Beaufort Sea with wind duration. (a) Scaling including all waves measured hourly by SWIFTs, with corresponding wind duration from Figure 3.1b. The least squares regression shown by the dashed line has a correlation of $R^2 = 0.02$. (b) Scaling using only duration-limited waves in open water from empirical screening. The least squares regression has an $R^2 = 0.002$. The definition of wind duration, shown here, is found to not be sufficient for describing the observed duration-limited growth.

includes duration for only measurements that were screened as likely to be duration-limited based on the minimum wind speed and open water distance determined by Figure 3.2 (52% of the total dataset). Wave energy does not scale well with wind duration for either dataset, with $R^2 = 0.02$ and $R^2 = 0.002$, respectively. This further confirms that spurious correlation is likely not the dominant mechanism in the distance-limited results, above.

3.4 Ice-limited conditions

Estimates of the portion of ice cover surrounding SWIFT drifters are shown in Figure 3.1c. Consistent with the onboard images from each buoy, ice cover was zero for the entirety of the SWIFT 11 deployment, and the majority of the SWIFT 10 deployment. Nonzero ice concentrations were calculated for SWIFT 15 in mid-August using the AMSR2, ranging from 0.01 to 0.61.

3.4.1 Data screening

In order to explore wave growth where the wave generation is ice-limited, we only use wave measurements where the ice concentrations qualitatively agree with the *in situ* image observations, waves are distance-limited according to the same criteria as used in open water, and where winds are blowing off-ice rather than on-ice, such that the presence of attenuated waves generated in open water is minimized (and wave generation can be studied in isolation). All of the ice concentrations for the SWIFT 15 record qualitatively agreed with SWIFT images. We found no waves in partial ice that qualify as duration-limited due to the short open water distances, but many that were classified as unsteady due to fluctuating winds (where unsteady winds are indicated by U_{10} changing by more than 0.12 m/s). Additionally, a number of these waves were formed in on-ice wind conditions such that only six wave measurements from SWIFT 15 are classified as distance-limited with off-ice winds.

Ice concentrations calculated for SWIFT 10 in early September using AMSR2, all less than 0.08, are in clear disagreement with the observations from SWIFT images, and are indicated in the figure by transparent red circles. We instead used concentrations from RS2

images collocated with SWIFT 10 on September 8 and 12, which agree well with the ice concentrations in the SWIFT images. Local concentrations were 0.12 and 0.11, respectively. These wave measurements were classified as duration-limited, and are in off-ice wind conditions. As a result, we identified a total of eight points as likely to be distance-limited in partial ice cover where reliable ice concentration estimates are available and winds are off-ice, indicated in Figure 3.1c by opaque points. Measurements for other non-zero ice concentrations are shown in Figure 3.1c by transparent points. The highest portion of ice cover observed for distance-limited waves was 0.61, near the beginning of the SWIFT 15 deployment, where significant wave height is 0.13 m.

3.4.2 Wave energy in ice

Wave and wind measurements in partial ice were used to calculate nondimensional wave energy. The relationship of nondimensional wave energy with ice concentration estimated from AMSR2 and RS2 for all measurements in ice is shown in Figure 3.5a. The exponential fit is poor, with a coefficient of determination of $R^2 = 0.06$. In comparison, Figure 3.5b shows the relationship of nondimensional wave energy with local ice concentration when generation of short, distance-limited waves in the ice is expected: winds are relatively steady, and blowing from the ice pack towards open water. Additionally, we only use ice concentrations where they are determined to be reasonable based on observations from SWIFT mast cameras. This shows a significant improvement over the inclusion of all nonzero ice concentrations. Using a simple least squares regression to a power-law, the coefficient of determination is now $R^2 = 0.82$, and the relationship is:

$$\tilde{E} = 1.95 \times 10^{-5} A^{-0.51} \tag{3.2}$$

Nondimensional wave energy measured in partial ice cover was used to estimate 'effective' nondimensional distance in ice ($\mathcal{X}_{ice}$) for the screened wave measurements by applying the fit of nondimensional distance and wave energy in open water, given by Equation 3.1. This approach gives the nondimensional 'effective fetch' that would place the observations in ice

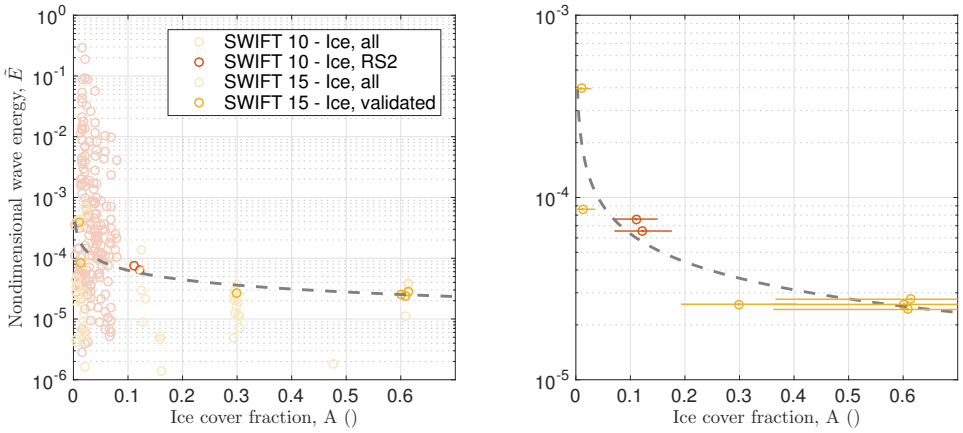

Figure 3.5: Exponential relationship of nondimensional wave energy, $\tilde{E}$ with local fraction of ice cover, A, for (a) all wave measurements in partial ice, and for (b) distance-limited wave measurements in off-ice wind conditions where ice concentrations have been validated with estimates from SWIFT images. Colors correspond to instruments as seen in Figure 1; transparent points correspond to measurements that were screened. Nondimensional wave energy is calculated using measured wave height and wind speed. Error estimates of ice cover fraction in (b) are the standard deviation of ice concentration values within a 30-km radius of SWIFT location.

along the same regression line as the observations in open water based on measured wave height and wind speed. (These points are shown as open circles on the black line in Figure 3.3.) Here, we use the results of the least squares regression fit to our open water field data, $\tilde{E} = A\mathcal{X}^a$, but fetch relations from the literature could be used in the absence of open water measurements. Equations 3.1 and 3.2 can then be combined to give 'effective' nondimensional distance in ice as a function of ice concentration:

$$\mathcal{X}_{ice} = 162A^{-0.49} \tag{3.3}$$

This comparison suggests that the 'effective fetch' rapidly decays with increasing ice fraction. These relationships are determined empirically, but can be used to predict waves where ice cover and wind speed are known. Figure 3.6 shows the prediction of resulting fetch-limited wave heights for this dataset.

Table 3.1: Summary of statistics for wave data sets from 2012 and 2014.

Data set	# measurements	Slope of fit	R^2
2012 – all	1247	1.35	0.56
2012 – open, distance	317	1.56	0.63
2012 – ice, distance	24	–[a]	–[a]
2014 – all	1680	0.88	0.64
2014 – open, distance	433	0.98	0.77
2014 – ice, distance	8	−0.49	0.82

[a]Fit was not calculated due to insufficient information on ice concentration.

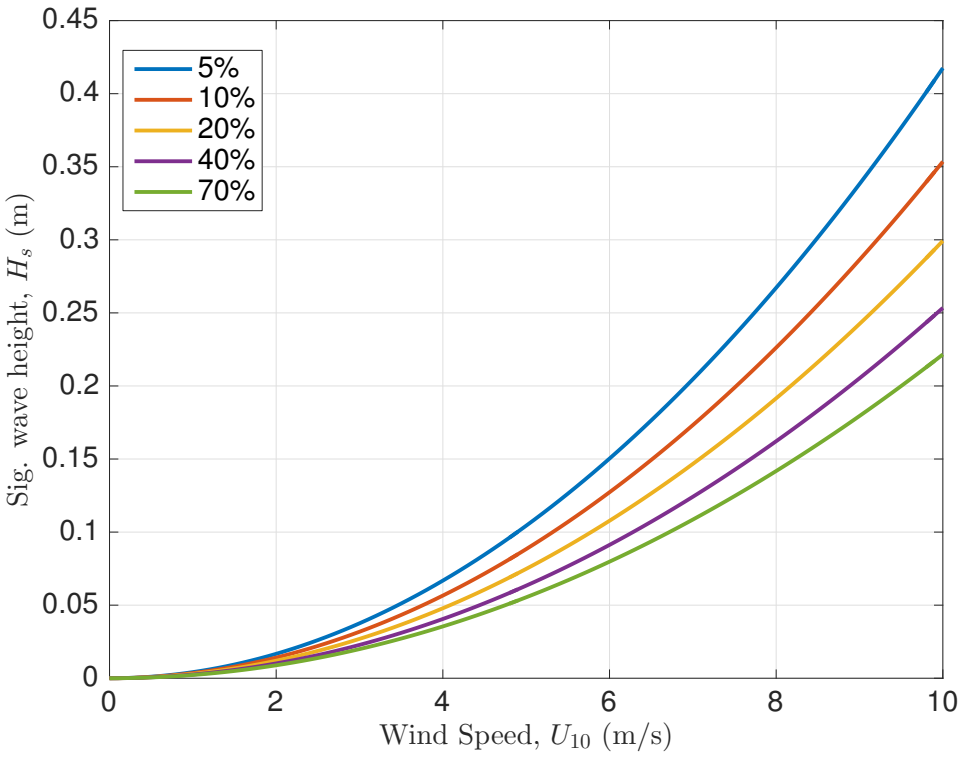

Figure 3.6: Simple model for predicting wave height of short fetch-limited waves generated in the MIZ given a wind speed and ice concentration. Curves for five ice concentrations are shown here (5%, 10%, 20%, 40% and 70%) with wind speeds from 0-10 m/s, but solutions can be determined for any ice concentration or wind speed with Equations 3.1 and 3.3.

Chapter 4

DISCUSSION

4.1 Wave evolution

The observed good correlation of the scaling of all open water wave measurements with distance, regardless of qualification as distance- or duration-limited, indicates that the basin scale is often a limiting factor in open water wave development (Figure 3.3a). In contrast, we observe that waves are rarely purely duration-limited (Figure 3.4), evidenced by the failure of commonly defined wind duration variables to capture duration-limited growth of waves. However, the improvement of the distance-limited scaling by screening waves for wind and wave stationarity does show a more nuanced dependence on open water distance and wind duration (and one which is more consistent with true fetch limitation). The distance-limited scaling would likely be further improved by screening rapid changes in wind direction or wind speed along the waves axis. These parameters are not considered here, but are incorporated in spectral wave models such as WaveWatch3 and SWAN.

The adherence to distance limited scaling laws is similarly seen in the scaling of nondimensional open water distance with nondimensional wave frequency (Equation 1.6), where there is an even stronger correlation of $R^2 = 0.87$ (Figure 4.1). The trend is fit by the equation

$$\nu = 4.0\mathcal{X}^{-0.33} \tag{4.1}$$

This result compares well with results from previous fetch limitation experiments, where the exponential fit is on average $\nu = 2.4\mathcal{X}^{-0.275}$ (Babanin and Soloviev, 1998). The nondimensional frequency can be seen as an analog for the inverse wave age, where wave age is $\frac{T_e g}{2\pi U_{10}}$ (T_e is energy-weighted average period and U_{10} is ten-meter wind speed, as earlier defined). The strong scaling of nondimensional frequency with nondimensional distance then indicates that

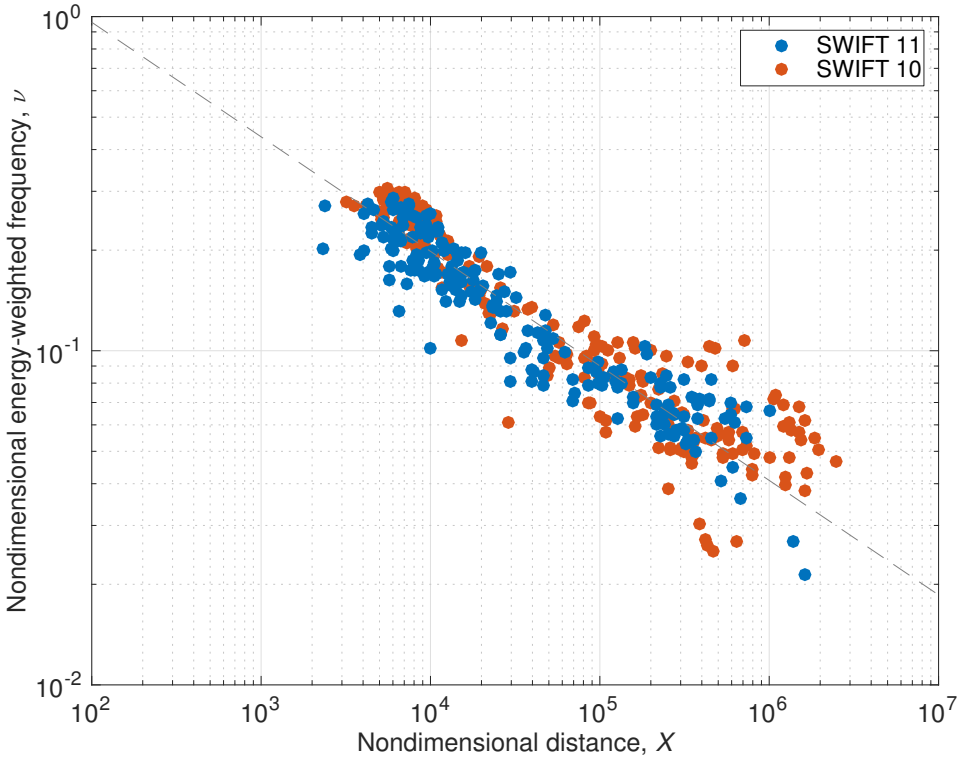

Figure 4.1: Scaling of waves in the Beaufort Sea, using nondimensional energy-weighted frequency versus nondimensional open water distance. Dashed line shows logarithmic regression to data with a slope of $\mathcal{X}^{-0.33}$, and coefficient of determination $R^2 = 0.87$.

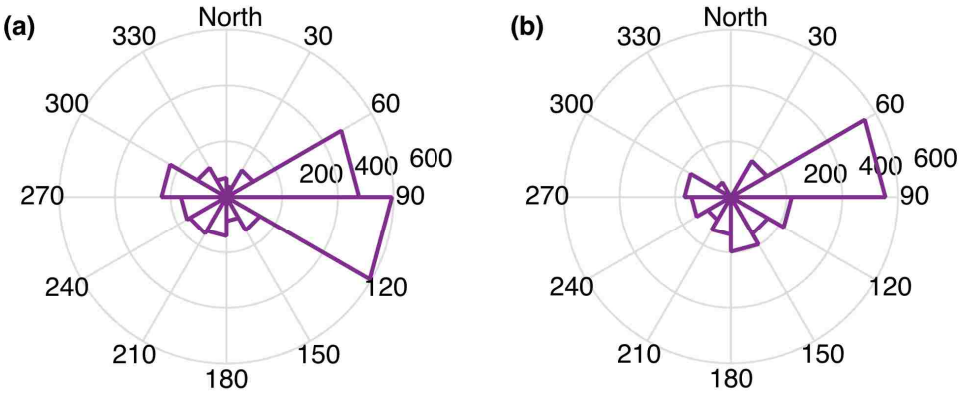

Figure 4.2: Rose diagrams of peak (a) wind and (b) wave directions from SWIFTs 10 and 11 when in open water areas. Directions are expressed as the direction from which winds or waves originate, with North at 0°.

older waves develop when longer open water distances are available. As the Arctic Ocean basin scale becomes larger with increased ice retreat, the wave field will likely be dominated by more mature swell waves.

As older swell waves are likely to have come from further away in the basin, we expect that they will correlate less with local wind conditions. In Figure 4.2, we show compass rose distributions of peak wave and wind directions during open water observations. The distributions are similar for waves and winds, but have noticeable differences, especially between 60° and 120° (from the east). In determining the nondimensional variables using the locally measured wind speed and direction, we make an implicit assumption that the wind is constant across the open water distance. However, at large open water distances such as most of those seen here, it is highly unlikely that winds are constant across the distance (Donelan et al., 1985). We expect that the older observed waves, at higher nondimensional frequencies, may be more likely to have local wind directions that are not aligned with the peak direction of the wave field. Yet, there is no significant correlation between wave age and the difference between wave and wind directions ($R^2 = 0.16$, not shown). Instead, it may be that they are more likely to be misaligned when winds are blowing at a large angle

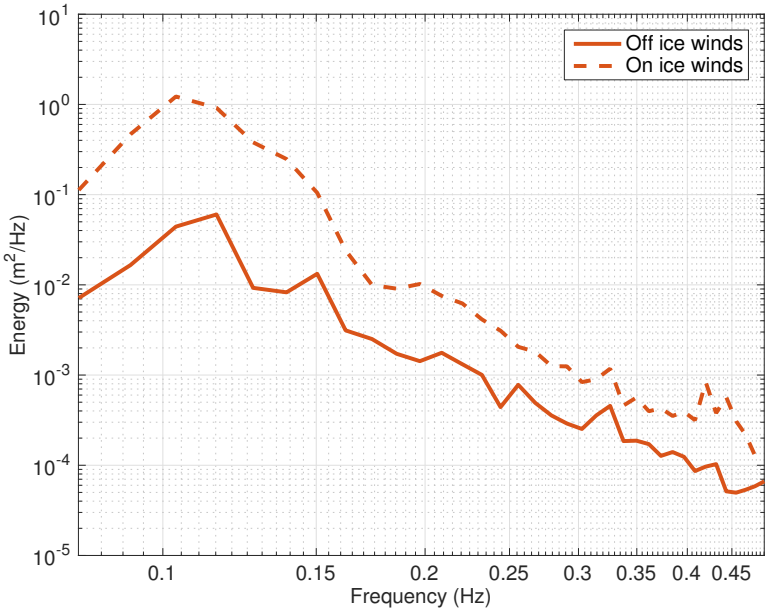

Figure 4.3: Wave spectral measurements from SWIFT 10 during off-ice wind conditions (solid line), where wave field is composed primarily of waves generated in partial ice cover by the 'effective fetch' between floes, and during on-ice wind conditions (dashed line), where wave signal is composed of both waves generated in partial ice and a low-frequency swell component from open water. Spectral measurements represent 3-hour averages from otherwise similar wind and sea ice conditions.

to the coastline. Thus, accounting for the relative angle of the wind to the coastline or ice edge will improve distance-limited wave predictions.

While the energy balance governing ocean waves in open water depends on winds, nonlinear interactions, and breaking dissipation, the presence of sea ice introduces scattering and additional dissipation, and may also alter the wind, nonlinear interactions, and breaking dependencies themselves (Li et al., 2015; Zippel and Thomson, 2016). The use of the 'effective fetch' between ice floes to describe waves generated in partially ice-covered ocean is quantitatively justified for bulk wave statistics, as the local equilibrium balance is approximately maintained (Zippel and Thomson, 2016), but is a simplification of the physical processes

that create the complex wave field of the marginal ice zone.

One such process, the attenuation of incoming waves by an ice field, is illustrated by comparing wave spectra generated by on-ice winds on September 14 (dashed line) and off-ice winds on September 5 (solid line). These spectra represent three-hour averages of wave measurements, and were chosen due to similarity in all conditions except for wind direction; average wind speed for both is 10.0 m/s, ice concentrations were qualitatively similar based on on-board SWIFT images, and average wind directions were respectively 331° and 71° (i.e., off-ice and on-ice with an east-southeast ice edge). Wave attenuation by sea ice is a well-described process resulting from on-ice wind and wave conditions; incoming short, high frequency waves are rapidly damped out such that the longer waves are able to penetrate furthest into the ice. Additionally, attenuation by damping and dissipation of waves in partial ice prevents the downshifting of energy. These processes are evident in the resulting two-dimensional wave spectra as a combination of high-frequency wind sea with low energy generated by local winds and a low-frequency swell component from attenuated incoming waves. In comparison, the wave spectra measured in off-ice winds has a similar shape at the high frequencies, as a result of local wind sea wave generation, but is lacking the low-frequency swell component and has lower energies overall. This shape is more similar to wave spectra observed in open water, and indicates that local wave generation is likely.

The damping of short waves by the ice field also causes the ocean to become less efficient at gaining energy from the wind by reducing the roughness of the surface (Zippel and Thomson, 2016). This feedback suggests that under the on-ice wind conditions observed in Figure 4.3, the increased energy at low frequencies from incoming swell aligned with the wind field contributes to the increased energy at higher frequencies. Swell aligned with wind may provide further opportunity for wave generation or recapturing of swell in wind sea. Under off-ice wind conditions, the isotropic and low energy wave field provides little opportunity for a substantial wave field to develop. This result confirms the findings of Masson and LeBlond (1989), that generation of a wave field in the MIZ is severely limited, but the extent to which this is true depends on the existing wave field and wave direction. Thus, the spectral

distribution of energy will depend highly on the wave history and basin scale when on-ice winds and waves exist, and primarily on the local wind stress, u_*, when winds are off-ice (Figure 4.3).

Additionally, the use of the 'effective fetch' to describe wave generation in partial ice cover assumes that the majority of the wave energy comes from wind blowing over patches of open water, and that the distances between floes will be relatively homogeneous for a given fraction of ice cover (i.e. Figure 1.4). Relevant distances for wave generation and attenuation at a given ice concentration will also depend on floe size distribution and geometry (Robin, 1963; Steele et al., 1989; Bismuth, 2016). Strong winds blowing over a thick sheet of sea ice has also been shown to be capable of generating waves in the ice, but of a small magnitude that can be considered negligible for the wind and wave conditions observed here (Crocker and Wadhams, 1988). The more relevant process for consideration in the MIZ is the re-radiation of wave energy by heaving ice floes. Floe-floe interactions in the MIZ can cause nonlinear transfers of energy and increased directional spread (Wadhams et al., 1986). These processes are complex and difficult to model, but are necessary to consider to predict the directional spectrum of waves in partial ice cover.

4.2 Sensitivity to ice products

We have shown a strong dependence of wave energy and frequency on open water distance as a function of ice extent in both open water and partial ice in the Beaufort Sea. However, the ability to make predictions based on these relationships depends on the accuracy of the ice product used. There are a number of ice products readily available online, and they vary in the methods for detecting the ice edge and thresholds for determining ice presence. Here, we have chosen to use the NIC IMS product for ice extent when measuring waves in open water and the University of Bremen AMSR2 product for ice concentration when measuring waves in partial ice cover, both of which utilize the ASI algorithm. These products were chosen based on product resolution, accessibility, and prevalence in relevant literature. Both methods have demonstrated skill at estimating ice coverage in the Arctic Ocean, and are capable of

detecting thin and deteriorating ice as they are composites of multiple ice detection methods.

However, the disagreement of both IMS and AMSR2 ice products with observed ice conditions from the SWIFT mast camera and RS2 images on a number of occasions indicates that a bias exists on the local scale. The error estimates of ice concentration (Figure 3.5) range from 2% at low ice concentrations to 24% at high ice concentrations. In partially ice-covered oceans, small changes in the fraction of ice cover can significantly impact both generation and attenuation of wave energy. A recently published discussion of sea ice concentration products shows that the bias of the ASI algorithm is relatively high compared to other algorithms (Ivanova et al., 2015). The atmospheric interference at this frequency from clouds, particularly common in the MIZ, provides a significant source of error. Predictions of waves in ice-covered oceans might be improved by using ice concentration algorithms such as Bristol or CalVal with relatively low bias and standard deviation (Ivanova et al., 2015). Nonetheless, scalings presented here of open water waves based on distances from both IMS and AMSR2 ice products are successful, supporting previous indications that these readily available ice products are sufficient for large-scale prediction of waves in ice-free areas of the Arctic Ocean.

4.3 Reanalysis of 2012 wave data

We have reanalyzed previously published 2012 data from the Beaufort Sea (Thomson and Rogers, 2014) by removing duration-limited waves and screening for distance-limited waves with conditions defined for our 2014 dataset. The applicability of fetch laws to open water distances in the Arctic Ocean was first shown with this 2012 wave data from a subsurface AWAC wave buoy moored at 75°N 150°W in the Beaufort Sea (Thomson and Rogers, 2014). The wave mooring provides a complete time series of wave characteristics, and wind speeds are obtained from the NAVGEM model. Ice presence is indicated by significant wave heights significantly below those predicted by the wave model, and increased roughness in the sea surface time series. More details of the data set can be found in Thomson and Rogers (2014).

The scaling of wave energy from the 2012 dataset is refined by the reanalysis, shown

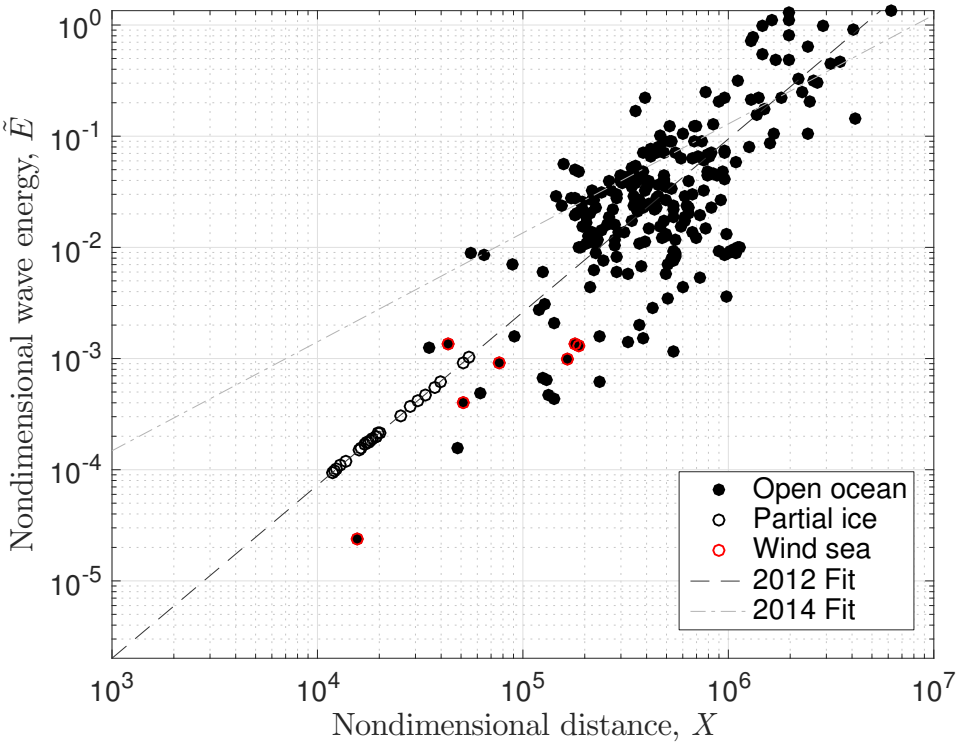

Figure 4.4: Scaling of waves in Beaufort Sea in 2012 at wave mooring in Beaufort Sea, 75°N 150°W, with nondimensional wave energy versus nondimensional open water distance. This scaling represents a reanalysis of the results presented in Thomson and Rogers (2014), by using the IMS ice product and screening out waves not classified as distance-limited. Dark dashed line is least squares regression for 2012 results shown, with a slope of $\mathcal{X}^{1.56}$, and light dot-dashed line is least squares regression from 2014 results, with a slope of $\mathcal{X}^{0.98}$. Points outlined in red are distance-limited waves that also classify as wind sea, with a wave age less than 1. Waves in partial ice for October 27 are shown as open circles that have been forced to the line to infer nondimensional distance, $\mathcal{X}_{ice}$.

in Figure 4.4. The original analysis of these data in Thomson and Rogers (2014) used a different ice product and did not screen duration-limited or unsteady waves to find a slope of $\mathcal{X}^{1.6}$ for the scaling of wave energy with open water distance. In our reanalysis, we first recalculate open water distance with the IMS ice product, reducing the slope to $\mathcal{X}^{1.35}$, and the R^2 to 0.50. Then, the screening of duration-limited and unsteady points excludes 73% of the data (see Table 3.1), and increases the R^2 to 0.57, with a slope of $\mathcal{X}^{1.56}$. A summary of the data set is presented in Table 3.1. Although identifying the distance-limited waves improves the coefficient of determination, the slope of the regression is much greater than that found from the 2014 results (Figure 4.4), and still falls outside the range of coefficients previously stated in the literature (Young, 1999).

Thomson and Rogers (2014) found the power-law fit to wind sea waves, where wave age c_p/U_{10} is less than one, to be in much closer agreement to the expected dependence found in the literature, with a slope of $\mathcal{X}^1$.When the same screening for wind sea waves is applied in addition to the distance-limited screening, only seven points are classified as both young and distance-limited (outlined in red in Figure 4.4). The dependence of these points is also closer to those in the literature, with a fetch dependence of $\mathcal{X}^{1.28}$. In both cases, young wind sea waves make up a small portion of the wave measurements; wind sea waves are 15% of the total record before the distance-limited screening, and only 3% after screening to isolate distance-limited waves.

Based on records from the National Ice Center (2008), the 2012 open water season in the Arctic Ocean had the lowest ice extent recorded. As duration limitation is more likely to occur in oceans with large open water area, the substantial ice retreat may have led to wave conditions less frequently limited by basin size. The method for isolating distance-limited waves developed empirically using the 2014 data set has limited utility for data from 2012, where wave age plays a larger role.

The moored buoy observed partial ice where surface roughness was increased for a total of two weeks during the ice retreat and advance periods. However, we found the AMSR2 product to be insufficient in 2012 for obtaining ice concentrations to estimate distances

associated with waves in ice. The AMSR2 product predicted a concentration between 0% and 100% only one day out of the fourteen believed to have partial ice. The ice product indicated rapid expansion of the ice cover at the buoy location from 0% to 100% in only two days, from October 26 to 28. The product predicted 58% ice concentration surrounding the subsurface wave buoy on October 27. As with 2014 wave measurements in partial ice, nondimensional wave energy of hourly wave measurements in ice is used to infer nondimensional open water distance for distance-limited waves by forcing them to lie on the best fit line, as shown by open circles in Figure 4.4. Nondimensional 'effective' open water distances in ice range from 1×10^4 to 5×10^4 (Figure 4.4).

Additionally, hourly wave measurements believed to be in 58% ice cover lie well above the line fit to nondimensional distance and ice concentration, in Figure 3.5. We hypothesize that the ice product poorly predicts ice concentrations during this record due, in part, to a difference in ice cover type, as these waves were measured during freezing conditions of ice advance. Wave spectra showed a high amount of damping at low frequencies (not shown), suggesting the possibility of shuga or frazil ice. This result illustrates the limitation of this method for sea ice types other than the brash ice identified in the 2014 measurements. A different relationship between ice cover and wave energy likely exists during ice freezing and advance.

Chapter 5

CONCLUSIONS AND FUTURE WORK

We have demonstrated a significant exponential relationship between the nondimensional wave energy and open water distances across the Beaufort Sea. Waves measured in both 2012 and 2014 in this region indicate that the hard ice edge limits fetch in a conventional manner. However, scatter in the dataset indicates that the ocean rarely behaves in a purely distance-limited manner, and will also be limited by wind duration. These results lead to a few key conclusions:

1. Wind duration estimates, as commonly defined, are not sufficient for describing duration-limited wave growth.

2. Wave energy and period scale well with open water distance estimates for fetch-limited wave growth.

   (a) Scaling is improved by removing duration-limited and unsteady conditions.

   (b) Cutoffs for screening for fetch-limited waves are not universal, and must be determined empirically for a given location and time period.

3. Fetch-limited wave generation in partial ice is a function of the ice concentration.

Wave field observations during this year may be indicative of the new trend for waves in the emerging Arctic Ocean; with decreasing ice cover predicted, we are likely to observe more wave energy. The substantial improvement of distance-limited results by screening for relatively stationary winds and waves suggests that the likelihood of distance limitation decreases later in the summer and may generally decrease with reduced ice extent.

The emergence of mature swell waves is notable, because these waves carry more energy flux (for a given height) and penetrate further into sea ice (e.g., Wadhams et al., 1988). Wave energy in the Beaufort Sea is also controlled by sea ice extent in areas of partial ice cover. As originally suggested by Masson and LeBlond (1989) we observed that wind in the marginal ice zone is capable of generating very short, fetch-limited waves. In an MIZ with off-ice winds, wave generation is then a local process: waves are never duration-limited and are largely controlled by the distance between ice floes. Ice concentration, though not a perfect physical indicator of distance between floes, can be successfully used to indicate an 'effective fetch'. However, ice concentration from readily available products should be used only when empirically validated and conditions are relatively stationary. When winds are on-ice, local generation of waves across the 'effective fetch' will be observed in addition to incident and attenuated waves from open water. The possibility of the generation or growth over larger fetches with a diffuse wave field is an area for additional future research.

Application of this result is limited by the ice products presently available, which are sufficient for determining large scale ice extent, but not for local ice concentration and distance between floes. Currently, wave forecasts in ice by WaveWatch 3 (WW3) simply scale inputs by the ice concentration. Our results can be used as a simple test for the magnitude of the model's wave growth in partial ice, though is limited by not accounting for floe size distribution. It is clear that the physics of short, distance-limited waves in ice will not be described solely by the ice concentration, and that physically accurate wave models will need to consider the interaction of waves and ice for wave scattering and regeneration. Additionally, the open water distance for wave generation in partial ice depends on the geometry of floes and floe size distribution. Efforts are currently being made to obtain better floe size distribution estimates from satellite images, which will serve to improve our understanding of wave generation in fractional ice cover (Zhang et al., 2015).

BIBLIOGRAPHY

Babanin, A. V. and Soloviev, Y. P. (1998). Field investigation of transformation of the wind wave frequency spectrum with fetch and the stage of development. *J Phys Oceanogr*, 28(4):563–576.

Beitsch, A., Kaleschke, L., and Kern, S. (2013). Amsr2 asi 3.125 km sea ice concentration data. digital media V0.1, Institute of Oceanography, University of Hamburg, Germany, //ftp-projects.zmaw.de/seaice/.

Benschop, H. (1996). Windsnelheidsmetingen op zeestations en kuststations: herleiding waarden windsnelheid naar 10-meter niveau. *Koninklijk Nederlands Meteorologisch Instituut Technical Report*, 188.

Bismuth, E. (2016). Interactions vagues-glace dans l'estuaire et le golfe du saint-laurent. *Masters Thesis, Université du Québec à Rimouski*.

Bretschneider, C. L. (1952). The generation and decay of wind waves in deep water. *Trans Amer Geophys Union*, 33:381–389.

CERC (1977). Shore protection manual. *U.S. Army Coastal Engineering Research Center*, 3 Volumes.

Crocker, G. B. and Wadhams, P. (1988). Observations of wind-generated waves in antarctic fast ice. *J Phys Oceanogr*, 18:1292.

Darbyshire, J. (1959). A further investigation of wind generated waves. *Dtsch Hydrogr Z*, 12:1–13.

Donelan, M. A., Hamilton, J., and Hui, W. H. (1985). Directional spectra of wind-generated waves. *P Roy Soc Lond A Mat*, 315(1534):509–562.

Ewans, K. C. (1998). Observations of the directional spectrum of fetch-limited waves. *J Phys Oceanogr*, 28:495–512.

Fetterer, F., Knowles, K., Meier, W., and Savoie, M. (2002). Sea ice index. *Boulder, Colorado USA: National Snow and Ice Data Center.*, page http://dx.doi.org/10.7265/N5QJ7F7W.

Fontaine, E. (2013). A theoretical explanation of the fetch- and duration-limited laws. *J Phys Oceanogr*, 43:233–247.

Hasselmann, K. (1960). Grundgleichungen der seegangsvoraussage. *Schiffstechnik*, 1(191-195).

Hasselmann, K. (1973). Measurements of wind-wave growth and swell decay during the joint north sea wave project (jonswap). *Dtsch Hydrogr Z*, 8(12):95.

Herbers, T. H. C., Jessen, P. F., Janssen, T. T., Colbert, D. B., and MacMahan, J. H. (2012). Observing ocean surface waves with gps-tracked buoys. *J Atmos Ocean Tech*, 29:944–959.

Hogan, T., Liu, M., Ridout, J., Peng, M., Whitcomb, T., Ruston, B., Reynolds, C., Eckermann, S., Moskaitis, J., Baker, N., McCormack, J., Viner, K., J.G. McLay, M. F., Xu, L., Chen, C., , and Chang, S. (2014). The navy global environmental model. *Oceanography*, 27(3):116–125.

Hwang, P. A. (2006). Duration- and fetch- limited growth functions of wind generated waves parametrized with three different scaling wind velocities. *J Geophys Res*, 111:C02005.

Hwang, P. A. and Wang, D. W. (2004). Field measurements of duration-limited growth of wind-generated ocean surface waves at young stage of development. *J Phys Oceanogr*, 34:2316–2326.

Ivanova, N., Pedersen, L. T., Tonboe, R. T., Kern, S., Heygster, G., Lavergne, T., Sorensen, A., Saldo, R., Dybkjaer, G., Brucker, L., and Shokr, M. (2015). Satellite passive microwave measurements of sea ice concentration: an optimal algorithm and challenges. *Cryosphere*, 9:1797–1817.

Kohout, A. L., Williams, M. J. M., Dean, S. M., and Meylan, M. H. (2014). Storm-induced sea-ice breakup and the implications for ice extent. *Nature*, 509:604–607.

Li, J., Kohout, A. L., and Shen, H. H. (2015). Comparison of wave propogation through ice covers in calm and storm conditions. *Geophys Res Lett*, 42.

Liu, P. C., Schwab, D. J., and Jensen, R. E. (2002). Has wind-wave modeling reached its limit? *Ocean Eng*, 29(1):81–98.

Martin, T., Steele, M., and Zhang, J. (2014). Seasonality and long-term trends of arctic ocean surface stress in a model. *J Geophys Res-Oceans*, 119.

Martin, T., Tsamados, M., Schroeder, D., and Feltham, D. (2016). The impact of variable sea ice roughness on changes in arctic ocean surface stress: A model study. *J Geophys Res-Oceans*, 121.

Masson, D. and LeBlond, P. H. (1989). Spectral evolution of wind-generated surface gravity waves in a dispersed ice field. *J Fluid Mech*, 202:42–81.

Mitsuyasu, H. and Rikiishyi, K. (1978). The growth of duration-limited wind waves. *J Fluid Mech*, 85(4):705–730.

National Ice Center (2008). Ims daily northern hemisphere snow and ice analysis at 1 km, 4 km, and 24 km resolutions. boulder, co: National snow and ice data center. Digital Media.

Robin, G. D. Q. (1963). Wave propagation through fields of pack ice. *P Roy Soc Lond A Mat*, 255(1057):313–339.

Sanders, J. W. (1976). A growth-stage scaling model for the wind-driven sea. *Dtsch Hydrogr Z*, 29:136–161.

Schwendeman, M. and Thomson, J. (2014). Wave breaking dissipation in a young wind sea. *J Phys Oceanogr*, 44:104–127.

Smith, M. M. and Thomson, J. (2016). Scaling observations of surface waves in the beaufort sea. *Elem Sci Anth*.

Squire, V. (2007). Of ocean waves and sea-ice revisited. *Cold Reg Sci Technol*, 49:110–133.

Squire, V., Dugan, J., Wadhams, P., Rottier, P., and Liu, A. (1995). Of ocean waves and sea-ice. *Annu Rev Fluid Mech*, 27:115–168.

Steele, M., Morison, J. H., and Untersteiner, N. (1989). The partition of air-ice-ocean momentum exchange as a function of ice concentration, floe size, and draft. *J Geophys Res*, 94(C9):12739–12750.

Stewart, R. W. (1961). The wave drag of wind over water. *J Fluid Mech*, 10:189–194.

Sverdrup, H. U. and Munk, W. H. (1947). Wind, sea, and swell: Theory of relations and forecasting. *Hydrographic Office Pub, U.S. Department of the Navy*, 601:44.

Thomson, J. (2012). Wave breaking dissipation observed with "swift" drifters. *J Atmos Ocean Tech*, 29:1866–1882.

Thomson, J. and Rogers, W. E. (2014). Swell and sea in the emerging arctic ocean. *Geophys Res Lett*, 14(9):3136–3140.

Wadhams, P., Squire, V. A., Dougal, D. J., Goodman, J., Cowan, A. M., and Moore, S. C. (1988). The attenuation rates of ocean waves in the marginal ice zone. *J Geophys Res-Oceans*, 93(C6):6799–6818.

Wadhams, P., Squire, V. A., Ewing, J. A., and Pascal, R. W. (1986). The effect of the marginal ice zone on the directional wave spectrum of the ocean. *J Phys Oceanogr*, 16:358–376.

Wang, X. L., Feng, Y., Swail, V. R., and Cox, A. (2015). Historical changes in the beaufort-chukchi-bering seas surface winds and waves, 1971-2013. *J Climate*.

Young, I. (1999). *Wind Generated Ocean Waves*, volume 2 of *Ocean Engineering*. Elsevier.

Young, I. and Verhagen, L. A. (1996). The growth of fetch limited waves in a water of finite depth. part 2. spectral evolution. *Coast Eng*, 29(79-99).

Zhang, J., Schweiger, A., Steele, M., and Stern, H. (2015). Sea ice floe size distribution in the marginal ice zone: Theory and numerical experiments. *J Geophys Res-Oceans*, 120(5):3484–3498.

Zippel, S. and Thomson, J. (2016). Air-sea interactions in the marginal ice zone. *Elem Sci Anth*, 4.